RSC Advances

This is an *Accepted Manuscript*, which has been through the Royal Society of Chemistry peer review process and has been accepted for publication.

Accepted Manuscripts are published online shortly after acceptance, before technical editing, formatting and proof reading. Using this free service, authors can make their results available to the community, in citable form, before we publish the edited article. This *Accepted Manuscript* will be replaced by the edited, formatted and paginated article as soon as this is available.

You can find more information about *Accepted Manuscripts* in the Information for Authors.

Please note that technical editing may introduce minor changes to the text and/or graphics, which may alter content. The journal's standard Terms & Conditions and the Ethical guidelines still apply. In no event shall the Royal Society of Chemistry be held responsible for any errors or omissions in this *Accepted Manuscript* or any consequences arising from the use of any information it contains.

ROYAL SOCIETY OF CHEMISTRY

www.rsc.org/advances

Lanthanum nickel alloy catalyzed growth of nitrogen–doped carbon nanotubes by chemical vapor deposition

John Anthuvan Rajesh and Arumugam Pandurangan*

Department of Chemistry, Institute of Catalysis and Petroleum Technology

Anna University, Chennai–600025, Tamilnadu, India

Abstract

Nitrogen–doped carbon nanotubes (N–doped CNTs) were synthesized by chemical vapor deposition using lanthanum nickel ($LaNi_5$) alloy as a catalyst and acetylene/ammonia mixture as the carbon/nitrogen (C/N) precursor. The effect of experimental parameters such as temperature and time on the structure and yield of N–doped CNTs were studied. Transmission electron microscopy studies showed that with the increase of growth temperature and time, the C/N solubility, outer diameter and internal compartments of N–doped CNTs were increased progressively. The optimal condition for the synthesis of N–doped CNTs was found to be 900°C and 20 min. The elemental mapping of the catalyst tip confirmed that an intermetallic compound of lanthanum and nickel governs the growth of N–doped CNTs. X–ray photoelectron spectra revealed that the N content of CNTs varied between 3.5 and 6.9 at.% by changing the growth temperature. Confocal Raman spectroscopy analysis showed that the degree of graphitization dependence on the N doping level of CNTs. The growth of N–doped CNTs through the $LaNi_5$ alloy catalysis was discussed on the basis of both surface and bulk diffusion mechanism. Finally, the effect of acid treatment on the N–content and electronic structure of as–synthesized samples was investigated. These acid treated N–doped CNTs are expected to be more suitable for electrochemical applications, such as supercapacitors and oxygen reduction reaction in fuel cells.

RSC Advances Accepted Manuscript

1. Introduction

The exceptional electrical properties of nitrogen–doped carbon nanotubes (N–doped CNTs) make them extremely promising for use in the nanoelectronic applications[1–3], as well as in other great potential applications such as, metal–free electrocatalysts for oxygen reduction reaction, dye–sensitized solar cells, lithium–ion batteries and electrochemical supercapacitors.[3–9]

Synthesis of N–doped CNTs has been achieved by arc discharge[10], magnetron sputtering[11] and chemical vapor deposition (CVD).[12] The most common method for the synthesis of N–doped CNTs is catalytic pyrolysis of N–containing compounds by CVD (CCVD), including microwave plasma enhanced CVD, aerosol CVD, injection type CVD and thermal CVD.[13–17] CCVD has proved to be a relatively more effective than others when aiming for mass production at a low cost. Various CVD growth conditions, such as, catalyst composition, reaction temperature and the amount of nitrogen concentration present in the reaction mixture are the deciding factors for nitrogen content in the synthesized CNTs. Amongst, catalyst composition plays an important role in the solubility of carbon and nitrogen species on the surface and/or in the bulk of the catalyst, resulting in the growth of various nitrogen concentration containing CNTs. Generally, transition metals (Fe, Co and Ni), supported catalyst and ferrocene are found to be very effective for the production of N–doped CNTs.[2, 7, 8, 10, 11, 13–17] An important factor in the CCVD synthesis of N–doped CNTs is the diffusion rate of nitrogen on the metallic catalyst. The improved amount of nitrogen solubility on the metal catalysts through both surface and bulk diffusion is significant for the growth of high N–doped CNTs.[17] In addition, the introduction of second metal (co–catalyst) into the catalyst can considerably increases nitrogen diffusion. This is mainly due to the synergic effect of the involved metals.[18]

RSC Advances Accepted Manuscript

Several research groups have studied the effect of bimetallic catalysts on the growth of N–doped CNTs. The results showed that the composition of the catalyst has a significant role on the yield, microstructure, nitrogen content and properties of the synthesized nanotubes.[17, 18, 19–23] However, the role of bimetallic catalyst on the growth and formation mechanism of N–doped CNTs, very few reports has been dedicated to the scientific society.[17, 18, 23] Therefore, comprehensive study is needed to understand the role of bimetallic catalyst on the growth and formation mechanism of N–doped CNTs.

The intermetallic alloys lanthanum–nickel ($LaNi_5$) and magnesium–nickel (Mg–Ni) has been used as catalysts to produce CNTs.[24, 25] Particularly, the $LaNi_5$ alloy was already reported to be an efficient catalyst for the growth of CNTs, carbon nanofibers and boron nitride nanotubes.[24, 26, 27] Although, the fundamental understanding of the influence of $LaNi_5$ alloy catalyst on the growth of nanotubes and nanofibers is still lacking. In our previous studies, we have been shown that the catalytic activity of $LaNi_5$ alloy towards the growth of nickel–filled CNTs (Ni–filled CNTs) and silicon carbide nanowires (SiC NWs) by CVD.[28, 29] In addition to that, we explained the fundamental understanding of the influence of $LaNi_5$ alloy catalyst on the growth of Ni–filled CNTs and SiC NWs. On this basis, N–doped CNTs were successfully synthesized over $LaNi_5$ alloy catalyst by changing the experimental parameters and the possible growth mechanism is elucidated. Also, the present work is give attention to study the influence of the $LaNi_5$ alloy catalyst on the growth, yield, structure and nitrogen content of the nanotubes.

To date, acid treatment technique has been used for N–doped CNTs to modify their surface chemistry and it is commonly believed that the modified N–doped CNTs will have more opportunities for practical applications. Very recently, Chen et al showed the enhanced catalytic activity of HNO_3 acid treated N–doped CNTs for oxidative dehydrogenation of propane.[30] Fu et

RSC Advances Accepted Manuscript

al studied the influence of acid treatment on N–doped multi–walled CNT (MWCNT) supports for Fischer–Tropsch performance on cobalt catalyst.[31] Liu et al studied the chemical durability of the N–doped CNTs under 1–M HNO_3 acid and stirred at 80°C.[32] The effect of the acid treatment on the structure and electrical conductance of the N–doped MWCNTs was also determined by Burch et al.[33] Jiang et al have demonstrated that functionalization of gold nanoparticles with a homogeneous distribution on acid treated N–doped MWCNTs.[34] Despite the effect acid treatment on the nitrogen content and electronic structure of N–doped CNTs is seldom studied.

In recent years, N–doped carbon materials are a major focus for the electrochemical applications such as oxygen reduction reaction (ORR) in fuel cells and supercapacitors. Literature reports demonstrated that ORR activity and supercapacitor performance are directly related not only to the total nitrogen amount, but to the various nitrogen species present in the graphitic network. In addition, the concentrations of pyridinic, pyrrolic and quaternary nitrogen groups contribute differently to ORR activity and capacitance values in supercapacitors.[35, 36] So, it is an important scientific phenomenon to synthesize certain nitrogen groups in a controlled manner, modify their electronic structure and determine the concentration of different N species for various electrochemical applications.

Herein, we present a CVD synthesis of N–doped CNTs by pyrolysis of acetylene/ammonia (C_2H_2/NH_3) mixture over $LaNi_5$ alloy catalyst. Besides, the tendency of carbon/nitrogen (C/N) solubility on the alloy catalyst has been studied as a function of growth temperature and time. The microstructures and N–contents of nanotubes were obtained by transmission electron microscopy (TEM) and X–ray photoelectron spectroscopy (XPS), respectively. These results indicate a synergism of surface and bulk diffusion of C/N atoms on

RSC Advances Accepted Manuscript

the $LaNi_5$ alloy catalyst possibly provides high N–content CNTs. Also, the effect acid treatment on the nitrogen content and electronic structure of N–doped CNTs is investigated.

2. Experimental section

2.1. Synthesis of N–doped CNTs

The horizontal CVD consisted of a quartz tube gas flow reactor of 1000 mm length and 30 mm diameter and a tubular furnace equipped with programmable temperature controller was utilized for the synthesis of N–doped CNTs. The synthesis method was similar to that described elsewhere[24] except in the introduction of NH_3 as the nitrogen source. In brief, a quartz boat loaded with 100 mg of $LaNi_5$ alloy (99.5%, metal basis, Alfa Aesar) catalyst was placed at the centre of a tube furnace. The average particle size of the $LaNi_5$ alloy catalyst was determined from the particle size distribution analyzer and found to be in the range of 2–6 μm. Pure nitrogen was introduced into the quartz tube at a flow rate of 200 ml/min for 10 min before the flow rate was decreased to 50 ml/min; The furnace was heated from room temperature to 550°C at a rate of 5°C/min with a flow of nitrogen gas (N_2) at 50 ml/min. On reaching 550°C, N_2 was switched to hydrogen gas (H_2) at 100 ml/min for 20 min to reduce the catalyst. Then, the furnace was subsequently heated up to the desired reaction temperature ranged from 800 to 950°C under a 50 ml/min N_2 flow. Once the desired pyrolysis temperature reached a constant C/N feedstock flow of 60 ml/min C_2H_2 and 120 ml/min NH_3 was introduced into the reactor. The effect of reaction time on the growth of N–doped CNTs was also studied at 10, 20 and 30 min under the same reaction temperature (900°C) and C_2H_2/NH_3 (60 ml min^{-1}/120 ml min^{-1}) flow rate. All pyrolysis was performed in a H_2 flow atmosphere at a rate of 30 ml/min. After 20 min of growth, the sample was cooled to room temperature under N_2 ambient. The yield of as–synthesized samples was calculated from the following formula,[19]

RSC Advances Accepted Manuscript

$$\text{Yield (wt.\%)} = [(m_t - m_c)/m_c] \times 100$$

Where, m_c and m_t are initial weight of the catalyst and total weight of deposited sample with catalyst, respectively. The as–synthesized samples were heated in air at 400°C for removal of the residual carbon.

2.2. Instrumentations

The average particle size of the $LaNi_5$ alloy catalyst and H_2 treated catalyst was determined by laser scattering particle size distribution analyzer (Zetasizer Ver. 6.20). The structure of N–doped CNTs was initially carried out on a JEOL JSM–5800 and Hitachi S4800 scanning electron microscopes (SEM) operated at 20 kV. TEM (JEOL 3010) equipped with energy dispersive X–ray analysis (EDAX, Oxford instruments) operated at 200 kV was used to study the microstructure and compositional analysis of the N–doped CNTs. XPS measurements were performed using an Omicron Nanotechnology ESCA Probe system with monochromatic Al Kα X–rays (energy of 1486.7 eV). Confocal Raman spectroscopy analysis of the N–doped CNTs was done with a WiTec GmbH, Alpha–SNOM CRM 200 confocal Raman microscope having a 514 nm laser as the excitation source. The nitrogen contents of the as–synthesized and acid purified samples were evaluated by an elementary analysis in a GmbH VarioEL V3.00 system.

2.3. Acid treatment on as–synthesized samples

After characterization the effect of acid treatment on the nitrogen content and electronic structure of as–synthesized N–doped CNTs was studied. The as–synthesized samples were suspended in 3M, 1:3 ratio of sulfuric acid (H_2SO_4) and nitric acid (HNO_3) mixture and refluxed for 12 h at 80°C. After that the samples were washed with distilled water and filtered for several times and then dried in hot–air oven at a temperature of 100°C.

RSC Advances Accepted Manuscript

3. Results and discussion

3.1. Effect of hydrogen gas treatment on $LaNi_5$ alloy catalyst

CVD is a general technique to produce N–doped CNTs by a direct catalytic pyrolysis of suitable C/N sources. In our experiments $LaNi_5$ alloy used as a catalyst, C_2H_2 and NH_3 were used as C and N sources, respectively. Typical growth system involved a catalyst reduction step and a growth step where a C and N species generated and diffused over the alloy catalyst, and then bamboo–like structure formation by means of precipitation. In general H_2 gas treatment used for reducing the metal catalysts.[24, 25] The average particle size of the $LaNi_5$ alloy catalyst and H_2 treated catalyst was determined from particle size distribution analyzer and the corresponding histograms are presented in Fig. 1a and b, respectively. It can be seen from that the average particles size of the $LaNi_5$ alloy catalyst and H_2 treated catalyst were fall in the range of 2–6 μm and 50–500 nm, respectively. These histograms confirmed that the $LaNi_5$ alloy particles were reduced to smaller particles after H_2 gas treatment.

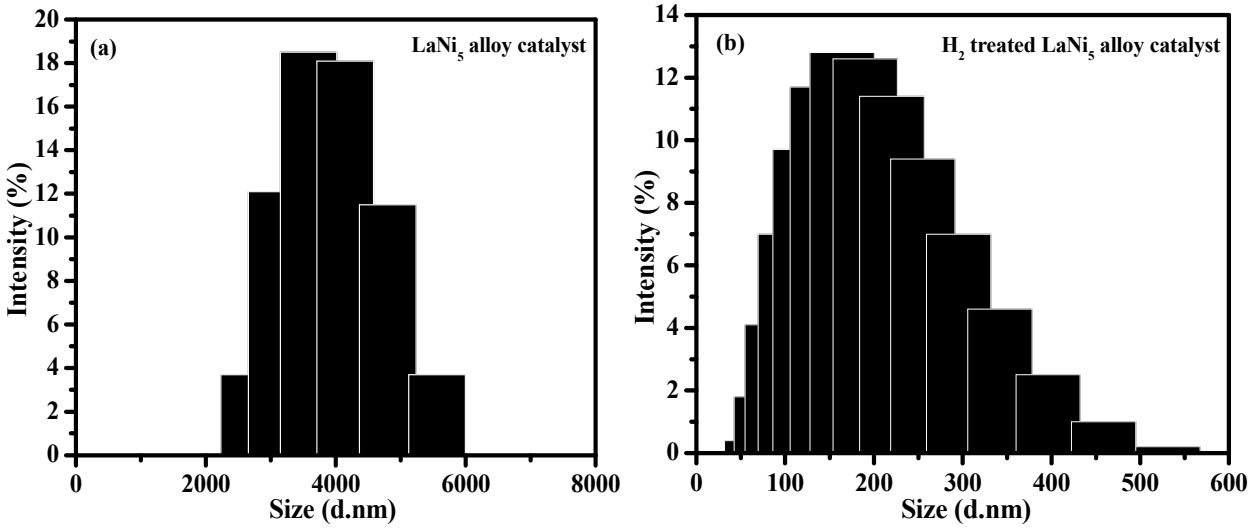

Fig. 1 – (a) and (b) particles size histogram of $LaNi_5$ alloy catalyst and H_2 treated $LaNi_5$ alloy catalyst for 20 min, respectively.

RSC Advances Accepted Manuscript

3.2. Effect of reaction temperature and time on the growth of N–doped CNTs (SEM observations)

The structure and yield of N–doped CNTs on $LaNi_5$ alloy was explored by systematically varying the growth temperature and reaction time. The experimental conditions such as reaction temperature and time on the synthesis and yield of N–doped CNTs on $LaNi_5$ alloy catalyst are summarized in Table 1.

Table 1 – Reaction conditions and yield of N–doped CNTs on $LaNi_5$ alloy catalyst.

Reaction conditions	Reaction temperature (°C)	Reaction time (min)	Yield (mg)	Yield (wt.%)
	800		330	214
Temperature	850	20	362	241
(°C)	**900**		**428**	**319**
	950		312	202
		10	361	239
Time	900	**20**	**428**	**319**
(min)		30	404	297

~100 mg $LaNi_5$ alloy catalyst used for every run.

Other experimental parameters are fixed and set as following: NH_3 flow rate, 120 ml/min; C_2H_2 flow rate, 60 ml/min; H_2 flow rate, 30 ml/min.

The yield of as–synthesized N–doped CNTs were increase with the increase in growth temperatures and found to be optimum at 900ºC, with further increase leads to decrease the yield (Table 1). A low yield was obtained for temperature at 800ºC, which is possibly due to the slow catalytic decomposition of NH_3. Increasing temperature increases N–doped CNTs yield and it

RSC Advances Accepted Manuscript

became significant at 900ºC. At higher temperature (950ºC), the catalyst particles rapidly agglomerates into bigger particles that are greatly initiate the growth of N–doped CNTs. However, the yield was greatly suppressed due to faster decomposition of C_2H_2 and NH_3 molecules have not enough time to adsorb on the catalyst surfaces.[37, 38]

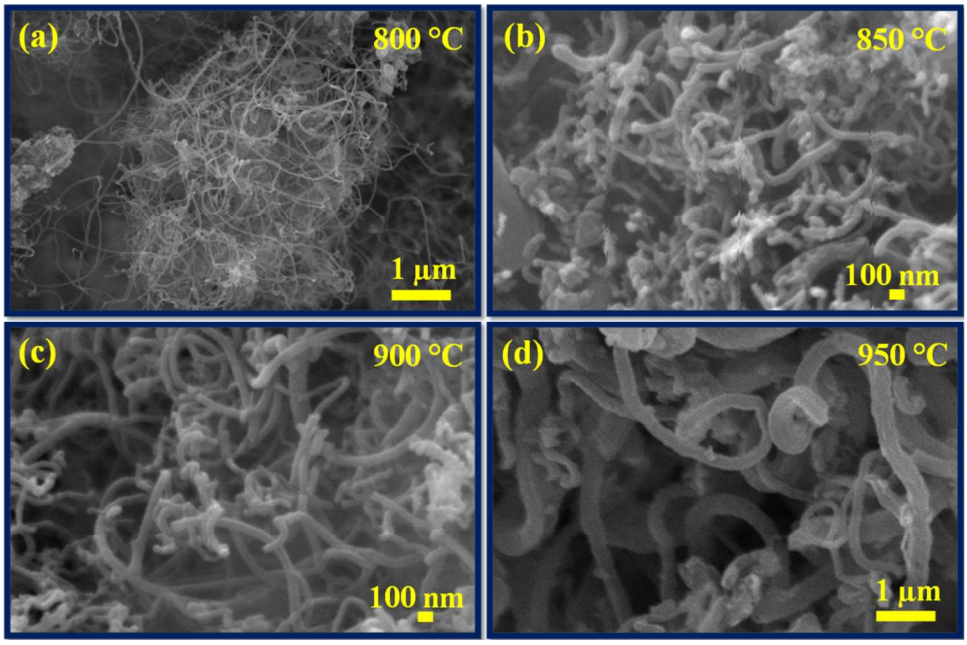

Fig. 2 – SEM images of N–doped CNTs synthesized at different reaction temperatures: (a) 800°C, (b) 850°C, (c) 900°C and (d) 950°C.

The synthesis temperatures on N–doped CNTs were significantly affected the diameter of the nanotubes as confirmed by SEM analysis. Fig. 2a–d shows the SEM images of N–doped CNTs grown under the same reaction time (20 min) and C_2H_2/NH_3 flow rate (60 ml min^{-1}/120 ml min^{-1}) but at different growth temperatures such as 800, 850, 900 and 950°C. It has been observed from that the average diameter of the nanotubes increases with temperature for the entire temperature range tested. The diameter distribution of synthesized N–doped CNTs at 800°C was uniform (Fig. 2a). As temperature further increases up to 900°C, the density and uniformity of N–doped CNTs considerably increased. It can be seen that at 900°C, Fig. 2c, the

RSC Advances Accepted Manuscript

nanotubes were packed more densely and have rather uniform diameter. A broad diameter distribution was obtained at 950°C, Fig. 2d, due to catalytic particles agglomeration. Temperature study suggests that the average diameter of the N–doped CNTs increase with increasing synthesis temperature from 800 to 950°C, which should result from the catalyst particles aggregation phenomenon.[37, 39] Moreover, the yield of N–doped CNTs tended to increase first and then decrease with increasing growth temperature (Table 1), the highest yield of 428 mg obtained for the growth temperature at 900ºC.

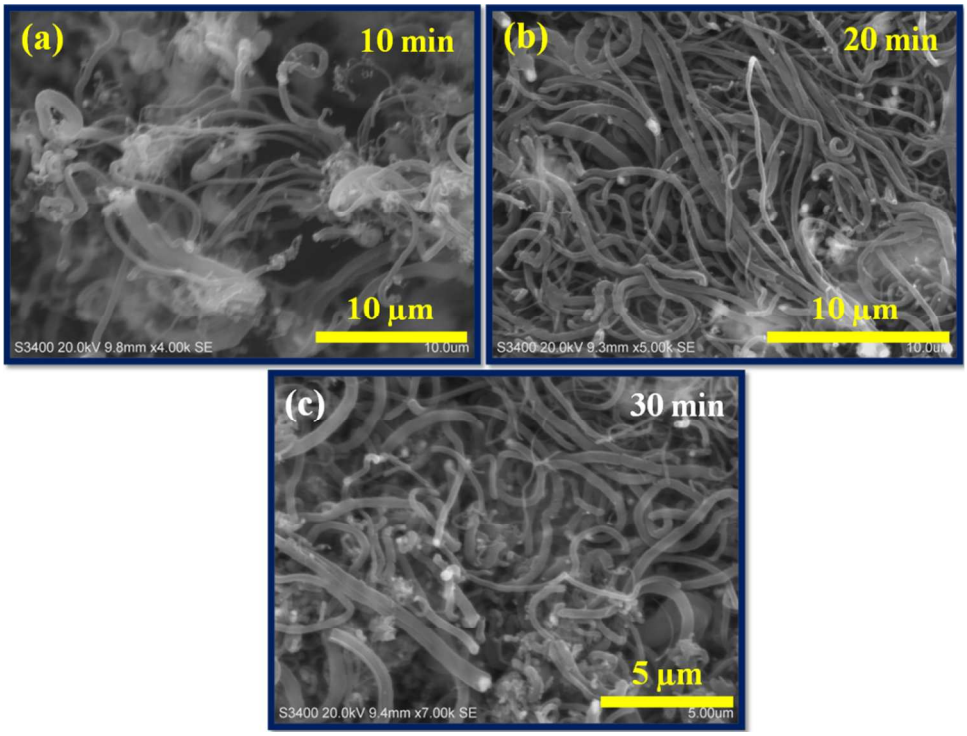

Fig. 3 – SEM images of N–doped CNTs synthesized at different reaction times: (a) 10 min, (b) 20 min and (c) 30 min.

Fig. 3a–c shows the SEM images of N–doped CNTs grown under the same reaction temperature (900°C) and C_2H_2/NH_3 (60 ml min^{-1}/120 ml min^{-1}) flow rate but at different growth times 10, 20 and 30 min. The results reveal that the synthesis time has an important factor on the

RSC Advances Accepted Manuscript

length of nanotubes. Considerable growth takes place during the 10 min of the reaction (Fig. 3a), then increased to reaction time at 20 min. The SEM image of nanotubes synthesized at 20 min growth time (Fig. 3b) shows the uniform diameter distribution and a length of over 10 micrometers. The nanotube length dropped at longer growth time (30 min), some thick and uneven nanotube diameters were found in the Fig. 3c. This is due to the increased C_2H_2/NH_3 feedstock flow concentration, which is consistent with the previous report by Koos et al.[14] The longer reaction time not only suppressed the length of N–doped CNTs also affect the yield of N–doped CNTs, which is shown in Table 1. The yield of as–synthesized N–doped CNTs at 10 min growth was about 361 mg, while at 20 min growth was about 428 mg. At 30 min growth, nanotubes yield was reduced to 404 mg. The reason for this is that increased NH_3 content may enhance the catalyst agglomeration, which leads to decrease in the nanotubes growth rate.[37] Therefore, the reaction time 20 min has the advantage for achieving the longest growth of nanotubes with high yield.

Data for synthesized N–doped CNTs diameters and lengths obtained from SEM images and the yields shown in Table 1 confirmed that the optimal reaction temperature and time for the synthesis of N–doped CNTs was 900°C and 20 min. The optimized conditions for better formation of N–doped CNTs are marked in bold letters (Table 1). In addition, the yield of the all as–synthesized samples produced using different reaction temperatures and time was above 300 mg, except only change in nanotubes diameter and length.

3.3. Transmission electron microscopy analysis

In order to investigate the relation between the catalyst, C/N solubility and diameter of the N–doped CNTs as a function of growth temperature and time, TEM analysis was carried out. Fig. 4 shows the TEM images of the N–doped CNTs synthesized at different reaction temperatures

RSC Advances Accepted Manuscript

such as 800, 850, 900 and 950°C. In overview the size of the catalyst particles were must be involved in the diameter and number of internal compartments in the nanotubes. From Fig. 4a–d, we can observe that the average diameter of the nanotubes and catalyst particles were increases with increasing temperature from 800 to 950°C.

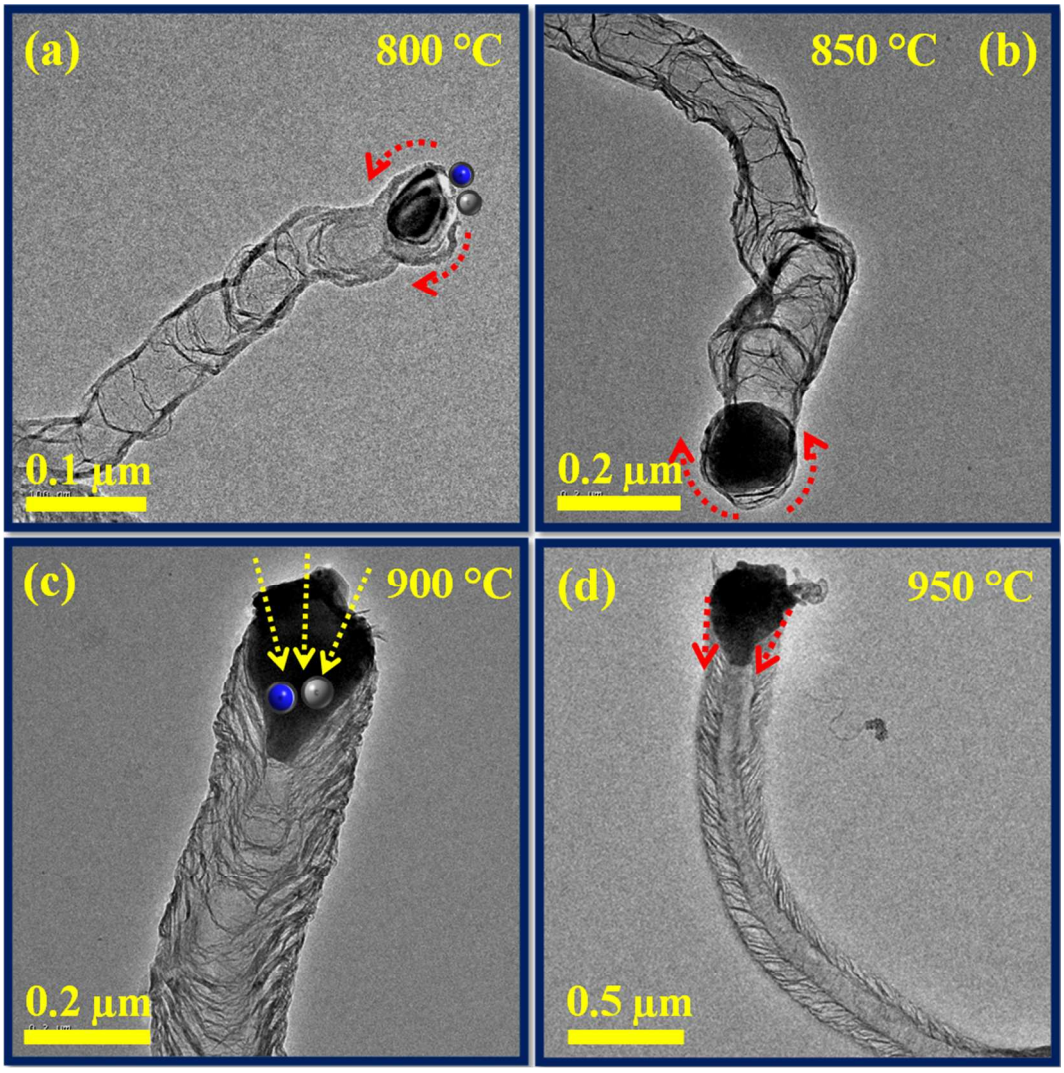

Fig. 4 – TEM images of N–doped CNTs synthesized at different reaction temperatures: (a) 800°C, (b) 850°C, (c) 900°C and (d) 950°C. The red and yellow dotted arrows are corresponding to surface and bulk diffusion of C/N atoms, respectively.

RSC Advances Accepted Manuscript

The outer diameter of N–doped CNTs synthesized at 800°C is around 70–80 nm, as seen in Fig. 4a. Further increases of reaction temperature to 850°C and 900°C, the outer diameter of N–doped CNTs increased to 160–170 nm and 190–200 nm, respectively, as shown in Fig. 4b and c. When the reaction temperature is increased to 950°C, the outer diameter of N–doped CNTs reached greatly to 240 nm (Fig. 4d). In addition, the definite particle size (round shape) observed by TEM was at 800 and 900°C, while at 900 and 950°C there are elongated particle size (polygonal shape), which should result from the particle agglomeration. This observation was consistent with SEM results. It is noteworthy that the C/N species solubility also increased with increasing reaction temperatures. Smaller sized particle (800°C) produced fewer internal compartments, while increased particle sizes (850 and 900°C) increases the amount of C/N solubility, which results in the formation of higher number of internal compartments and corrugated graphitic sheets. On the other hand, solubility of C/N species on the catalyst particle through bulk diffusion than surface diffusion increases the inner layers. These results suggest that the diameter of the nanotubes and solubility of C/N species are directly related to the diameter of the catalyst particles and the reaction temperatures, respectively.

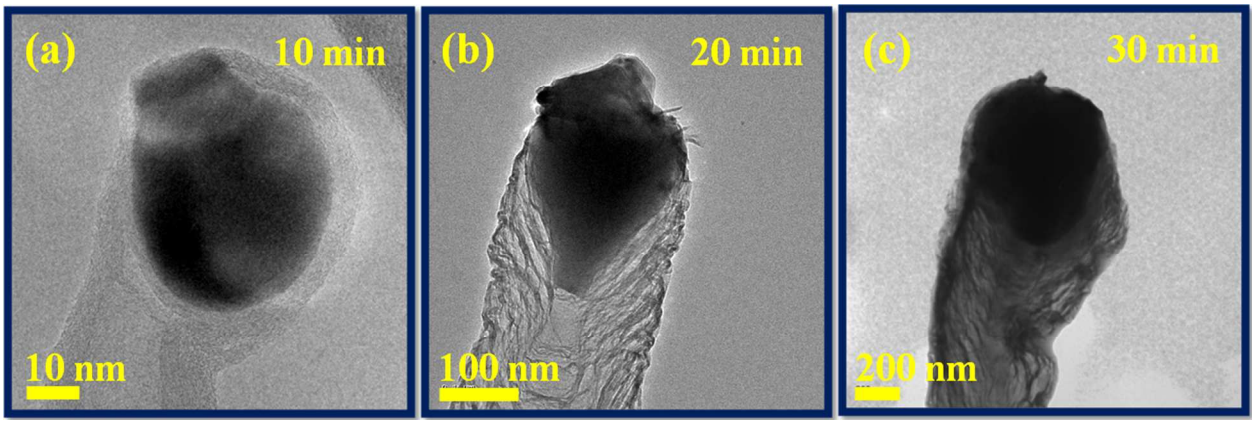

Fig. 5 – TEM images of N–doped CNTs synthesized at different growth times: (a) 10 min, (b) 20 min and (c) 30 min.

RSC Advances Accepted Manuscript

The tendency of C/N species solubility on the catalyst particles as a function of the growth time is also presented in Fig. 5. The increase of growth time from 10 to 30 min not only increases the C/N solubility also increases the size of the catalyst and diameter of the nanotubes. At growth time of 10 min (Fig. 5a) shows the clean and very low amount of C/N dissolution but at longer growth times (20 and 30 min) a drastic increase of C/N dissolution, which is result in the high transverse carbon bridges forming internal compartments (Fig. 5b and c). The more details about the relation between catalyst particles and C/N solubility are discussed in the later growth mechanism section. From the TEM analysis, it is clear that not only the diameter of the nanotubes increased at longer growth time (30 min) and higher reaction temperature (950°C) but also that the nanotubes get inhomogeneous structure (Fig. 4d and 5c). Therefore, the reaction temperature 900°C and growth time 20 min are taking advantage to produce good quality N–doped CNTs. Fig. 6a–c shows the three different TEM images of N–doped CNTs synthesized at optimized reaction condition (900°C and 20 min). It can be seen that all nanotubes exhibit bamboo–like structure with average diameter of 180–200 nm. In addition, regular internal compartments were observed inside the nanotubes and were terminated by end caps.

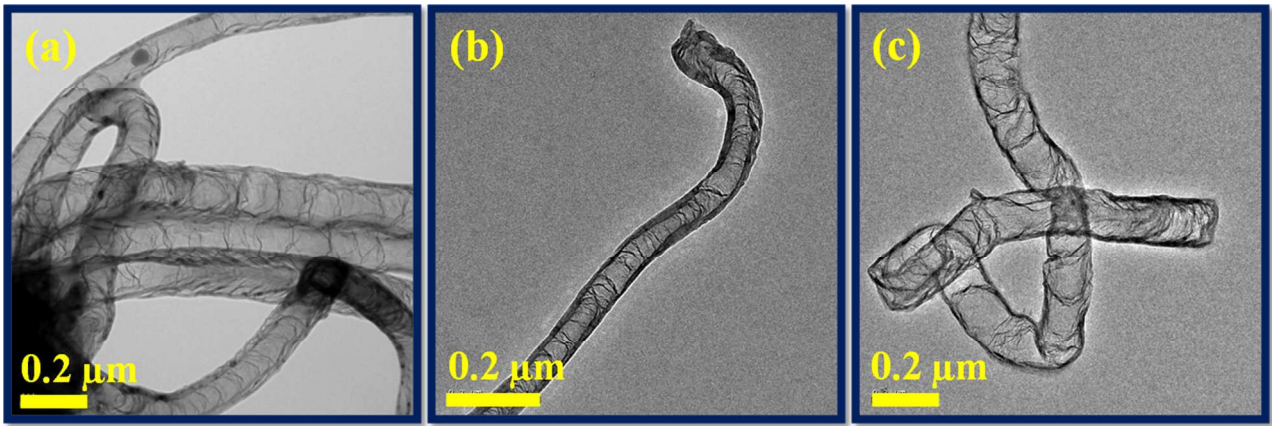

Fig. 6 – (a–c) TEM images of N–doped CNTs synthesized at optimized growth temperature and time of 900°C and 20 min, respectively.

RSC Advances Accepted Manuscript

Detailed structure of the individual N–doped CNTs was carried out with TEM and selected–area electron diffraction (SAED) analyses. The low magnification TEM image of the longest individual N–doped CNTs presented in Fig. 7a shows linearly interlinked periodic structures inside the nanotube with closed end by a hemi–fullerene cap. In overview, a packed array of parallel and imperfect linkages of the bamboo–like internal compartments exists inside the nanotube. As can be seen, the transverse carbon bridges forming internal compartments increase gradually along the tube direction (indicated by black arrows), as well as wall thickness.

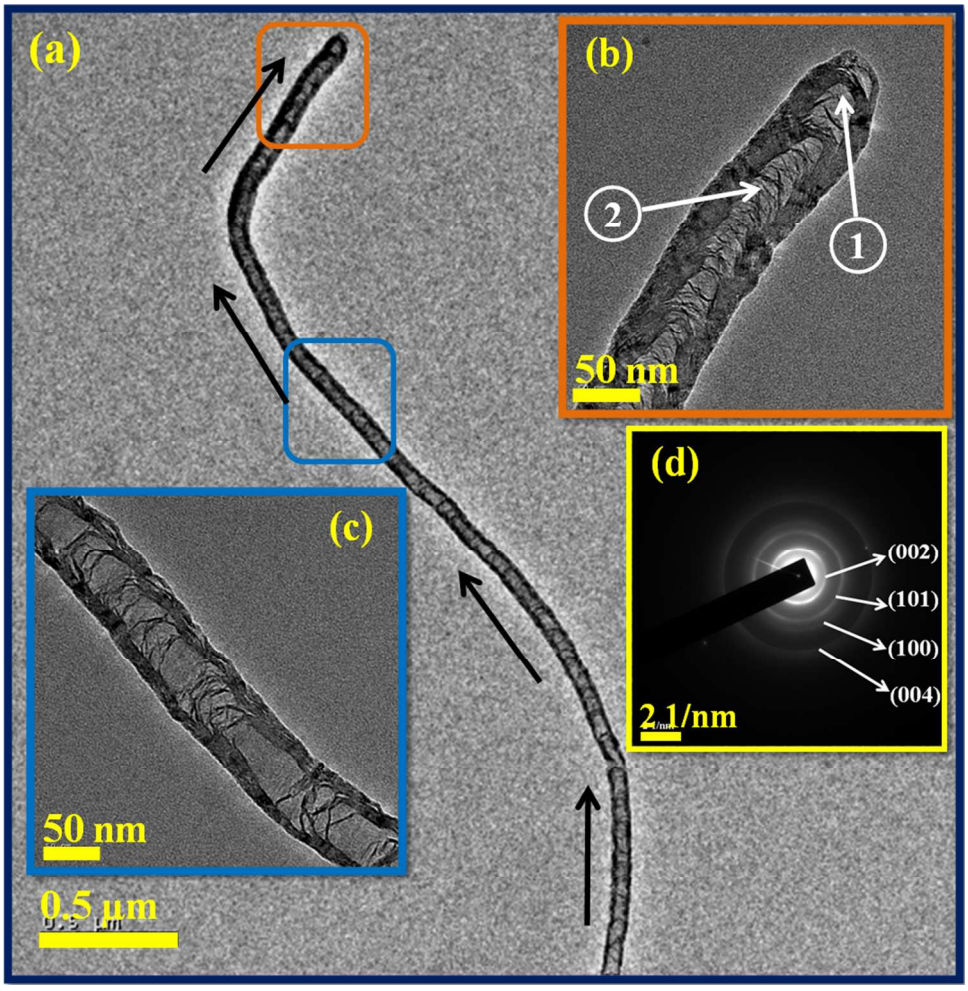

Fig. 7 – TEM images of (a) longest individual N–doped CNTs at low magnification; (b), (c) high magnification images of centre tube and closed cap end; (d) SAED pattern.

RSC Advances Accepted Manuscript

The higher magnification TEM images taken from the centre and end cap of the tube (squared regions) as shown in insets of Fig. 7b and c clearly indicate that a number of repeated internal compartments and thickness of the nanotube wall increased in the end cap region than in the centre of the region. It suggests that the characteristic structure of the tube depends on the nitrogen concentration; we believe that pyridine–like N–doping is responsible for both increased wall thickness and internal compartments. The selected area electron diffraction (SAED) pattern of N–doped CNT also in the inset of Fig. 7d, shows the strong (002) ring and other three diffuse rings (101), (100) and (004) planes of the graphite.

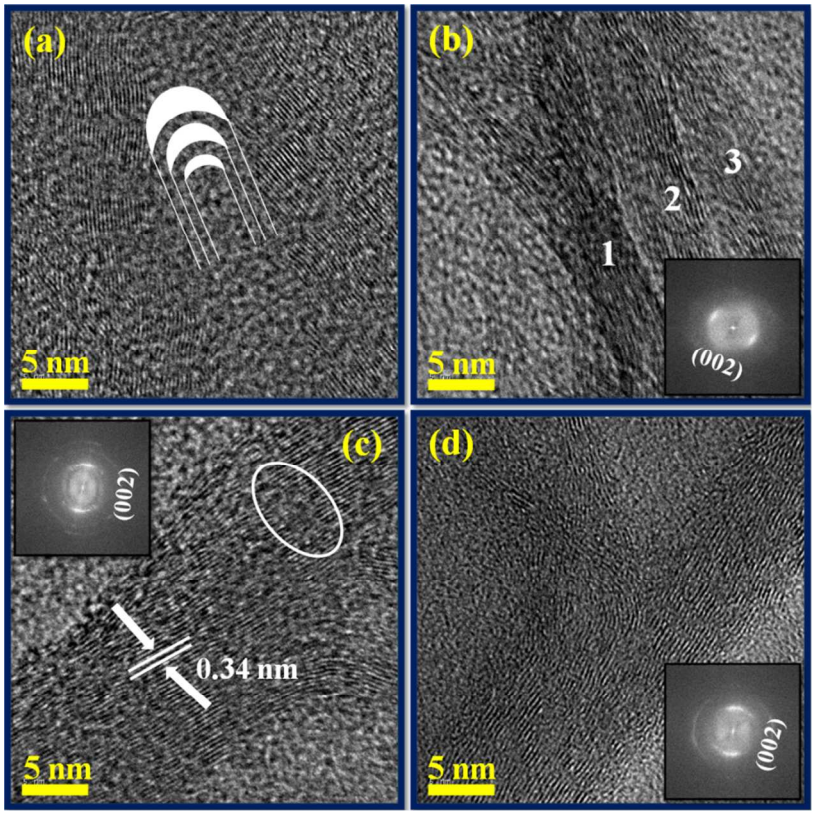

Fig. 8 – HRTEM images of (a) closed end cap region with a sketch shows the orientation of the graphene layers and closure of the system; (b) internal compartments of tube centre region, inset power spectra (FFT); (c), (d) graphitic layers of side wall nanotube and their insets were corresponding FFTs.

RSC Advances Accepted Manuscript

The atomic level structure and crystallinity of the N–doped CNTs were examined by HRTEM together with Fast Fourier transform (FFT). Fig. 8a and b are the atomic resolved HRTEM images of the closed cap and centre of the internal compartments (indicated by arrows 1 & 2 in Fig. 7c). In general, N–doped MWCNTs consist of nitrogen incorporated carbon hexagonal networks, which are concentrically rolled one another, and terminated by end caps. The closed cap structure was elucidated by considering pentagons and hexagons arranged in networks in which the nitrogen containing pentagons can induce curvature, resulting in the closure of the tube end. A sketch in Fig. 8a shows the orientation of the graphene layers and closure of the system. Atomic resolved HRTEM image taken from the centre of the tube (Fig. 8b) shows the continuous internal compartments marked by 1, 2 and 3. For such a typical unit, it is clear that the continuous three ropes of the internal compartments and one of them shows branched compartments. The corresponding FFT in inset shows the plane of (002) of graphite.

Fig. 8c and d were the atomic resolved HRTEM images of the side walls of the nanotube clearly show the multi–walled nature. It can be seen that the side walls are clearly connected with internal layers, resulting in the formation of internal compartments. The insets show the corresponding FFT of the HRTEM images showing the (002) plane of the graphite. The atomic layers in the walls are parallel to each other, with an interplanar spacing of 0.34 nm, which was closer to the interplanar spacing of the (002) plane of MWCNTs. Some defective graphitic sheets were also observed in the outer surface of the walls (circled in Fig. 8c). It is noteworthy that discontinuous lattice sheets, due to the incorporation of nitrogen atoms, resulted in the formation of holes or gaps.

RSC Advances Accepted Manuscript

3.4. X–ray photoelectron spectroscopy analysis

The total nitrogen content and nature of nitrogen atoms bonded in the CNTs were determined by XPS. Fig. 9a, d, g and j show the survey scan XPS spectra of N–doped CNTs synthesized at 800, 850, 900 and 950°C, respectively. The main peaks at 284.5, 400 and 532 eV correspond to C 1s of sp2 C (graphitic carbon), N 1s of the doped N and O 1s of the absorbed oxygen, respectively. The deconvoluted C 1s spectrum of N–doped CNTs (Fig. 9b, e, h and k) shows three different peaks C1 at 284.4, C2 at 285.6 and C3 at 287.6 eV. The strongest C1indicats that carbon was mostly present in the form of graphite–like sp^2 C, and the lower peak C2 corresponds to the C–N bond (N–sp^2 C). The weakest C3 resulting from the different bonding such as C≡N, C═O.[40] Fig. 9c, f, i and l show deconvoluted N1s XPS spectra of all samples display two main peaks N1 (pyridinic–like N) at 398 eV and N2 (graphitic–like N) at 400 eV. Our N 1s peak deconvolution is consistent with previous results on the N–doped CNTs.[2, 16, 20, 21, 40] The N concentration, defined as N/(C + N) atomic ratio%, was estimated by the area ratio of the N 1s and C 1s peaks and the calculated atomic percentage of N in the samples were about 3.5, 5.3, 6.9 and 4.1 at.% for 800, 850, 900 and 950°C, respectively.[2, 7] It can be seen that the total N content in the nanotubes increases with increasing growth temperature from 800 to 900°C, due to the decomposition rate of NH_3 and diffusion of N atoms on the catalyst increased gradually. At high growth temperature of 950°C, the N content was reduced to 4.1 at.%. There are two possible reasons proposed for the decrease of total N content at higher growth temperature. First, the bond energy of C–N (305 kJ/mol) is lower than that the C–C bond energy (370 kJ/mol), therefore C–C bond formation is more favorable than C–N bond at higher growth temperature. Second, generation of N_2 molecules from the pyrolysis of NH_3 left out from the reaction zone at higher growth temperature, decreases the total N content.[37]

RSC Advances Accepted Manuscript

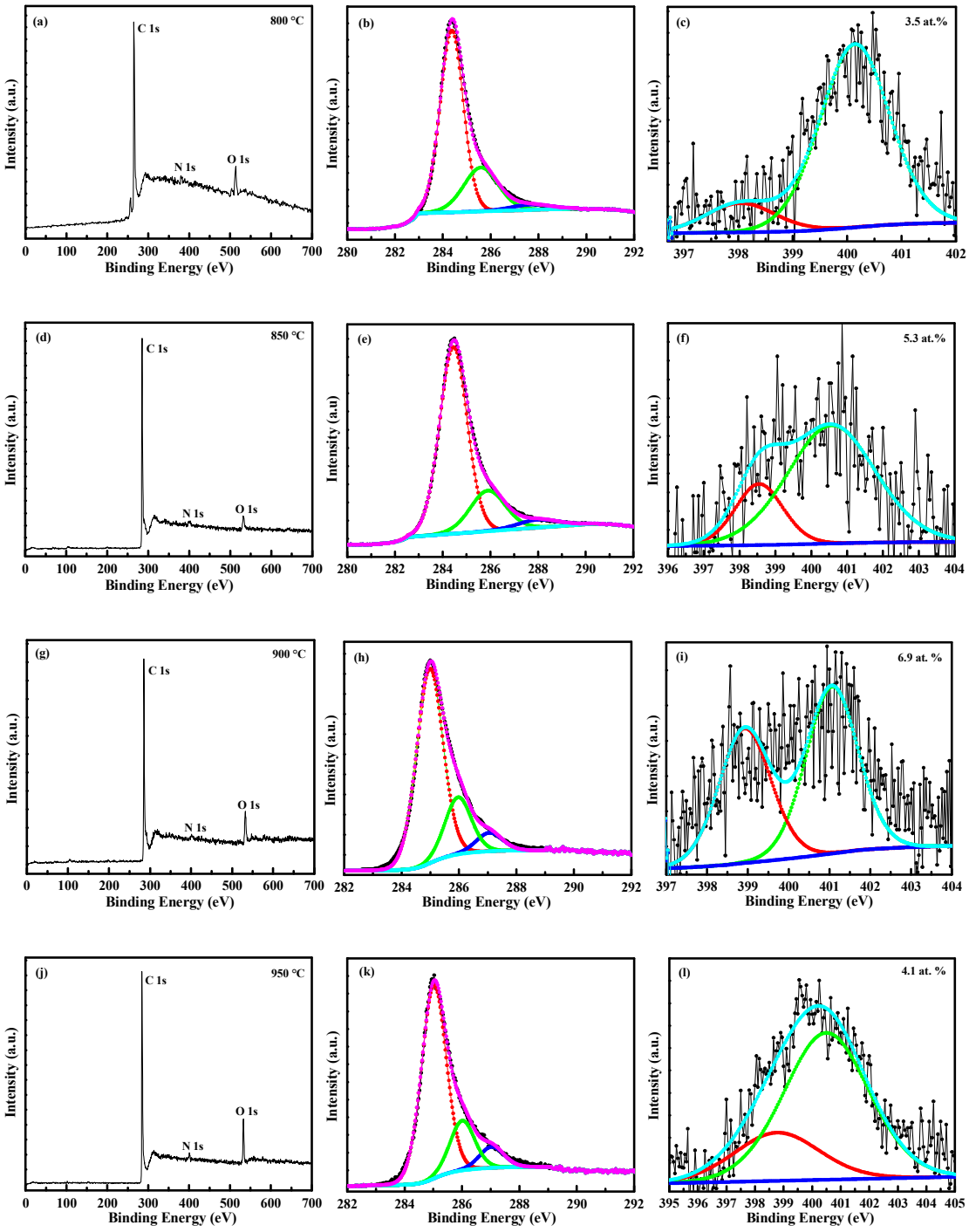

Fig. 9 – (a, d, g, j) wide scan XPS spectra, (b, e, h, k) deconvoluted C 1s spectra and (c, f, i, l) deconvoluted N 1s spectra of N–doped CNTs grown at 800, 850, 900 and 950°C.

RSC Advances Accepted Manuscript

Table 2 – Summary of N1s peak analysis on N–doped CNTs.

Temperature (°C)	Nitrogen moieties	B.E. (eV)	Area (%)	Graphitic N (at.%)	Pyridinic N (at.%)	Total N content N/(N+C) (at.%)
800	N1	398.1	14	3.0	0.5	3.5
	N2	400.1	86			
850	N1	398.5	22	4.1	1.2	5.3
	N2	400.5	78			
900	N1	398.2	33	4.6	2.3	6.9
	N2	400.3	67			
950	N1	398.7	25	3.1	1.0	4.1
	N2	400.4	75			

The results of the N 1s peak analysis are summarized in Table 2. The content of the pyridinic and graphitic N calculated from the relative area of corresponding N 1s XPS spectra constituents indicate that all nanotubes contain more graphitic N than pyridinic N while the ratio of these types (gN/pN) decrease from 6 to 2 with the increase of growth temperature up to 900°C. But at higher growth temperature (950°C), gN/pN ratio was increased to 3.1. Moreover, the proportion of pyridinic N also tends to increase up to 900°C and then decreased, which is contradictory to the previous literature report.[39] The possible reason is that the increasing growth

RSC Advances Accepted Manuscript

temperature transformed the N diffusion on the catalyst from surface to bulk diffusion, which resulted in increase of both total N and pyridinic N content and the highest N content was obtained as high as 6.9 at.% at 900°C. As the proportion of pyridinic–N increases, the number of internal compartment layers increase inside the nanotubes. These results are confirmed by TEM observations, as shown in Fig. 4a–c indicate that the corrugated structure of graphitic sheets and the internal compartments were increases from the growth temperature 800 to 900°C. Thus, the higher N containing CNTs (900°C) showed highly wavy like structure and internal compartments (Fig. 4c). The more details about the surface and bulk diffusion of N atoms on the $LaNi_5$ alloy catalyst is discussed on the growth mechanism section.

3.5. 2–D confocal Raman spectroscopy analysis

Raman spectroscopy was used to evaluate the degree of structural ordering present in the N–doped CNTs. The first– and second–order Raman spectra of N–doped CNTs synthesized at different growth temperatures are compared in Fig. 10. The spectrum shows two main peaks around 1360 cm^{-1} (D–band) and around 1580 cm^{-1} (G–band) corresponding to the first order Raman peaks. The additional peak located around 2700 cm^{-1} (G'–band) is traditionally referred to as second order Raman peak. There are many factors, which can affect the position of the D and G'–bands, such as doping of heteroatom[8], layer numbers[41], defects[42] and impurities.[43] In the present study, doping of nitrogen affected the intensity of the first order (D–band) and second order (G'–band) Raman peaks.

Fig. 10a–d show the Raman spectra of N–doped CNTs synthesized at different growth temperatures from 800 to 950°C, which determine the level of graphitization present in the nanotubes containing different content of N. It can be seen from that the increasing N–doping content from 3.5 to 6.9 at.% (800 to 900°C), the disorder induced first order Raman intensity

RSC Advances Accepted Manuscript

increased and the corresponding second order Raman intensity decreased. The I_D/I_G ratio of the N–doped CNTs was increased from 0.76 to 0.91, while the intensity ratio of $I_{G'}/I_G$ decreased from 0.73 to 0.63. Such a trend in the intensities suggests that doping level of nitrogen increased as a function of growth temperature, which can leads to the structural defects in the nanotubes. At higher growth temperature 950°C, the I_D/I_G ratio and $I_{G'}/I_G$ ratio was found to be 0.85 and 0.69, respectively. This indicates that the degree of crystalline perfection slightly increased, which is due to reduced N–doping content (4.1 at.%). Therefore, Raman results concluded that the level of defects is related to the amount of N–doping in the CNTs.

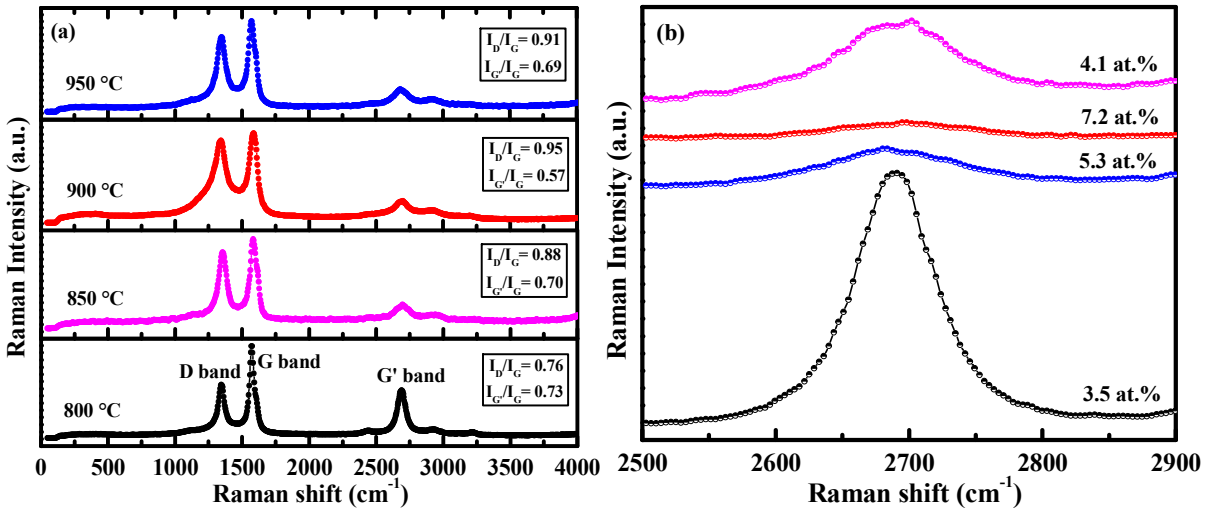

Fig. 10 – (a) Confocal Raman spectra of N–doped CNTs synthesized at different growth temperatures: 800, 850, 900 and 950°C and (b) enlarged G' band spectra.

We used scanning confocal Raman microscopy for the first time to find information regarding the N–doping and crystallinity present in the individual N–doped CNTs. Fig. 11a shows the spatially resolved 2–D Raman image of single N–doped CNTs synthesized at 900°C and its corresponding Raman spectra collected from the marked regions 1, 2 and 3 presented in Fig. 11b. It can be seen from the marked regions 1–3, that when the disorder induced first order Raman intensity increased, the corresponding second order Raman intensity decreased. The I_D/I_G

RSC Advances Accepted Manuscript

ratios of the Raman spectrum increased from the marked regions 1–3 were ~0.91, ~0.93 and ~1.04, while the intensity ratio of $I_{G'}/I_G$ decreased from the marked regions 1–3 (~0.80, ~0.73 and ~0.68). This result suggests that the disorder introduced by the N atoms were doped with various concentrations at these three different regions via both graphitic and pyridinic types. In addition, the average intensity ratio of I_D/I_G and $I_{G'}/I_G$ were calculated to be 0.96 and 0.74, respectively, which are relatively consistent with the result of bulk N–doped CNTs (0.95 and 0.57).

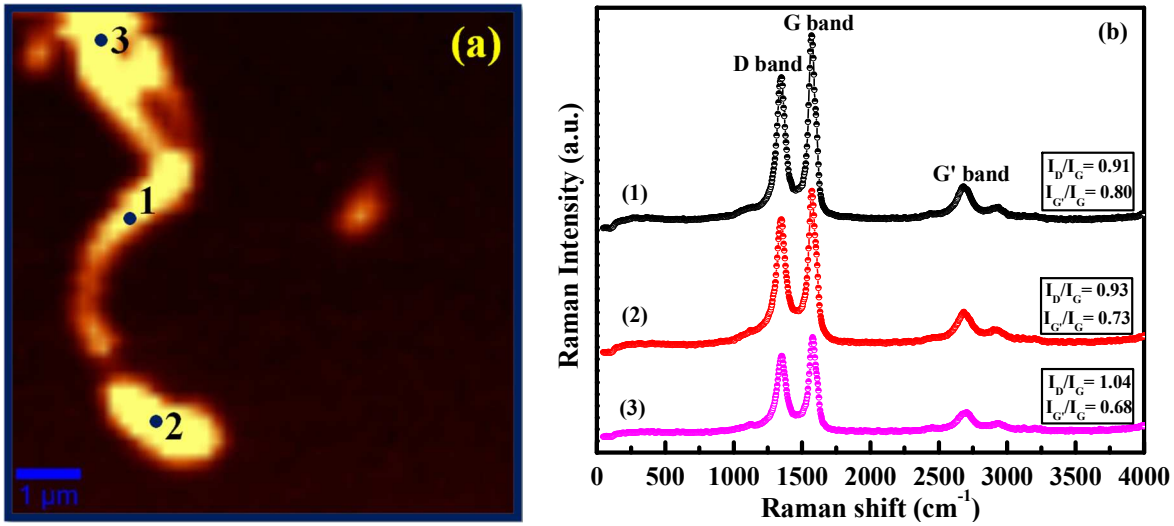

Fig. 11 – (a) 2–D confocal Raman image of individual N–doped CNTs; (b) Raman spectra collected from the points marked regions 1, 2 and 3.

3.6. Growth mechanism (energy dispersive X–ray analysis)

To develop a better understanding of the composition and growth process, the EDAX spectrum and elemental mapping were taken to examine the individual N–doped CNTs grown from a catalyst particle as shown in Fig. 12a. Fig. 12d displays the EDAX spectrum of N–doped CNT embedded with catalyst particle, which exhibits the presence of C, N, La and Ni. The nanotube is primarily carbonaceous and is composed of C and N species, while Ni is the dominant composition of the attached catalyst particle. The observed copper signal in spectra originated

RSC Advances Accepted Manuscript

from the supporting TEM copper grid used. The EDAX elemental mapping of the catalyst at the top of the nanotube is shown in Fig. 12b and c. The scanning result indicates that the catalyst particle is composed of Ni (yellow) and La (blue). We inferred that the catalyst particle consists of an intermetallic compound of Ni and La governs the growth of the nanotubes.[24]

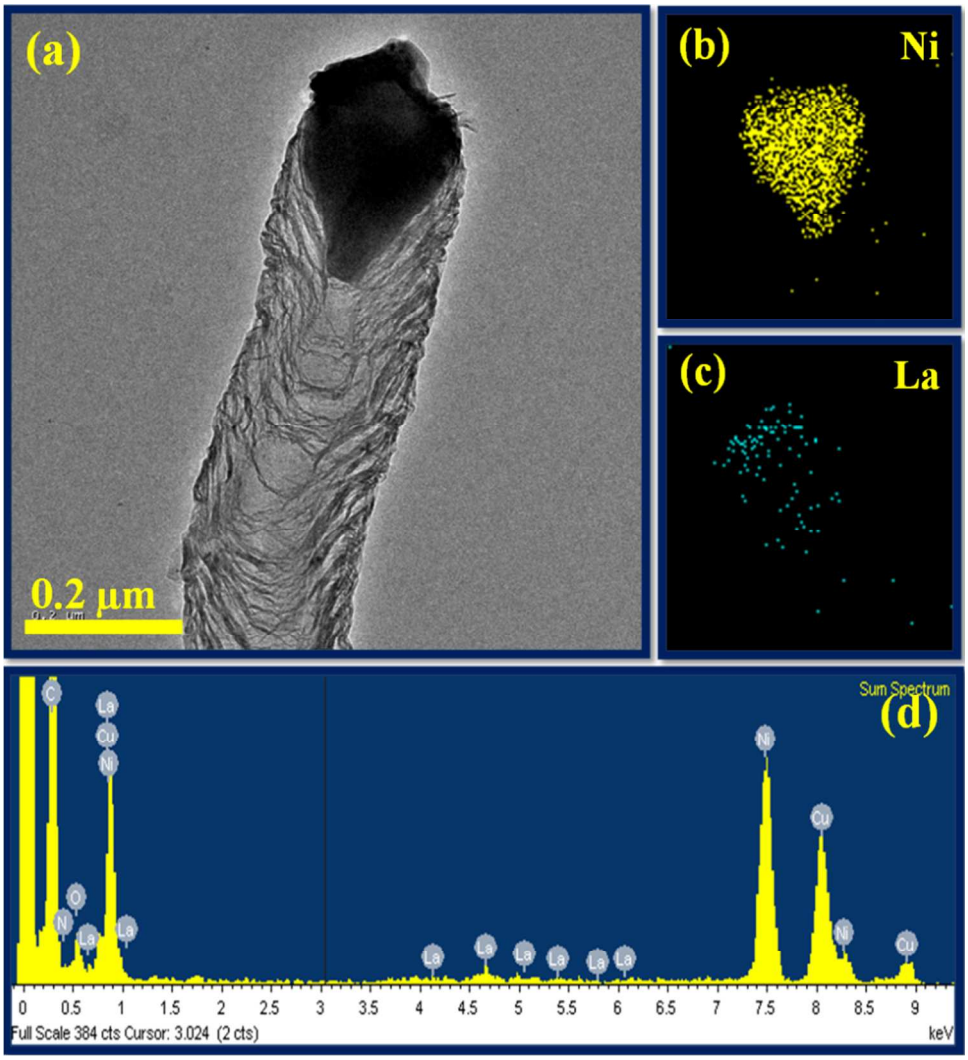

Fig. 12 – (a) TEM image of individual N–doped CNTs grown from a polygonal catalyst particle; (b, c) EDAX elemental mapping of catalyst tip; (d) EDAX spectrum collected from the nanotube shown in 12a.

RSC Advances Accepted Manuscript

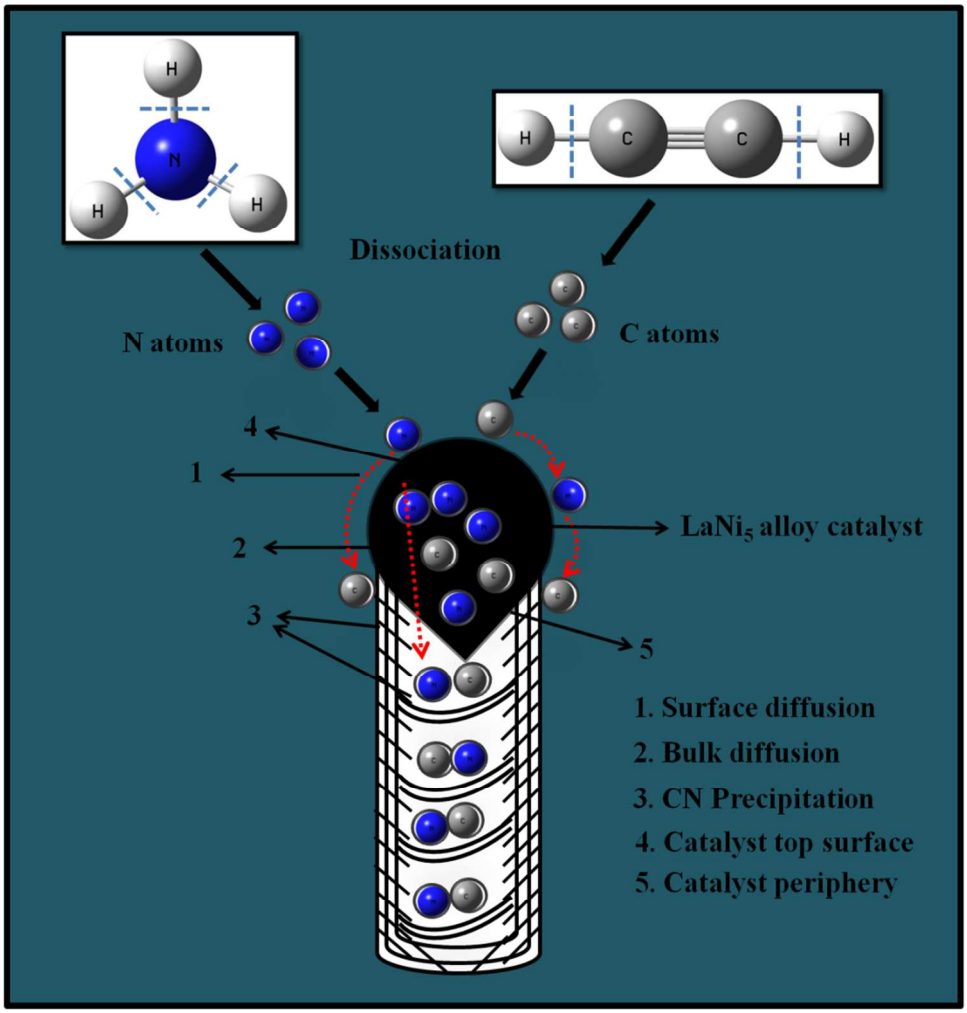

Fig. 13 – Schematic representation of N–doped CNTs growth through surface and bulk diffusion on $LaNi_5$ alloy catalyst.

To date, a number of different growth models related to the influence of catalyst and the growth of N–doped CNTs have been proposed.[17, 18, 23, 38, 44–47] However, a common feature observed in CCVD synthesis of N–doped CNTs is strong correlation between catalyst composition and nitrogen concentration.[11, 16, 18–23, 38, 44–47] This is explained in terms of different diffusion rates of CN or N species on the various catalysts. According to previous studies, there are two pathways such as surface and bulk diffusion of C/N species on the catalyst is needed for the growth of N–doped CNTs.[17, 44–49] Amongst, the bulk diffusion rates and higher saturated

RSC Advances Accepted Manuscript

concentration of N species in a catalyst provides highly N–doped CNTs.[17, 49] Based on this hypothesis and our TEM observations, we depict schematically the surface and bulk diffusion of C/N atoms on a $LaNi_5$ catalyst particle, as shown in Fig. 13.

Generally, our synthesis method was similar to the growth of pristine CNTs by CVD on $LaNi_5$ alloy catalyst.[24] Initially, the precursor molecules (C_2H_2/NH_3) were dissociated into C and N atoms by pyrolysis and then absorbed on the surface of the catalyst. Adsorbed atoms were diffused over the catalyst through surface or bulk and then dissolved on the catalyst. Finally, C/N atoms were precipitated on the opposite surface of catalyst and forms N–incorporated graphitic layers. The internal compartments of N–doped CNTs are formed by diffusion of C/N atoms on the top surface of the catalyst via bulk diffusion, while the side wall layers produced through surface diffusion on the both sides of the catalyst.[44, 46, 47] In our case, growth of N–doped CNTs happened by both surface and bulk diffusion on the catalyst through concurrently or alternatively. These explanations are confirmed by TEM observations and the contribution of surface and bulk diffusion of C/N atoms on the catalyst is marked in the Fig. 4a–d by dotted red and yellow arrows, respectively. In addition, their comparative involvement depends on the reaction temperatures and size of the catalyst particles.

At lower temperature (800°C) of smaller catalytic particle direct the dominant surface diffusion than bulk diffusion due to slower precipitation rate and has enough time to adsorb on the whole surface of the catalyst (Fig. 4a). Thus, C/N atoms were wrapped on the surface of catalytic particle highly and prevent the bulk diffusion. Therefore, nanotubes were doped with low N content of 3.5 at.%. With increasing growth temperatures (850 and 900°C) increase the size of the catalyst particles as well as precipitation rate. Hence, the catalytic envelop was reduced at 850°C, while at 900°C insignificant (Fig. 4b and c). This indicates that the diffusion

RSC Advances Accepted Manuscript

of C/N atoms changed from surface to bulk at 900°C and possibly gives higher N content (6.9 at.%). But at too higher reaction temperature (950°C) and larger catalyst particle size have faster precipitation rate. At the same time, formation of stable N_2 molecules (instead of atomic N) from the decomposition of NH_3 gets out from the reaction zone and hold down the diffusion of N species, which leads to decrease of N–doping. In Fig. 4d, it can be found that there are no internal compartments, which also probably decreases the N–content. This is mainly due to the precipitation of C/N species occurred on tilted surface (periphery) rather than the top surface of the catalyst. Therefore, the highest growth temperature is unfavorable for the growth of N–doped CNTs via bulk diffusion in our case. The same trend also happened by changing the growth time from 10 to 30 min. These results are once again confirmed by TEM observations, as shown in Fig. 5a–c. At growth time of 10 min and smaller size catalyst are obliging for surface diffusion while increased growth times (20 and 30 min) and larger size catalyst are in support of bulk diffusion. According to the above discussion, we concluded that our alloy catalytic method could contribute the both bulk diffusion and surface diffusion to the growth of N–doped CNTs depending on the growth temperatures and time.

Based on the TEM investigations (growth temperature and time study), we consider that the shape of catalytic particles mainly influences the formation of N–doped CNTs by modifying the reactants diffusion from surface to bulk. The reaction temperature has a significant role on the shape of catalyst particles. The catalysts particles tended to adopt a spherical shape at lower reaction temperatures 800 and 850°C, which resulted in graphitic carbon envelope and lower number of internal compartments. The shape of the catalytic particles changed from spherical to polygonal at higher growth temperatures (900 and 950°C) is responsible for the formation of

RSC Advances Accepted Manuscript

segmented graphitic sheets. As the catalytic particle shape changed, new active sites formed along their periphery. Consequently, C/N species diffusion happened on their periphery too.

Since the iron based (Fe) catalyst is widely used for the growth of N–doped CNTs than the Ni based catalyst.[2, 7, 8, 12–18, 20, 22, 37, 39, 40, 45, 47, 49] This is mainly due to continuous diffusion rate of N or CN atoms on the iron catalyst, whereas, in the case of Ni catalyst, N diffusion cannot but CN species may be diffuses over the catalyst surface.[50] Ni containing alloy catalysts and metal oxides were developed for the growth of CNTs with high purity and high yield.[24, 25, 51] The addition of La or Mg (adjuvant elements) into the Ni (active catalyst) helps to form an alloy structure possessing a lower melting temperature than the highest melting temperature of its constituents (Ni) and promotes solid–state reactions by forming ternary phases. Interestingly, a rare earth metal, La has been reported to show a catalytic effect for synthesizing single–walled CNTs and it was utilized as a catalytic promoter for synthesizing double–walled CNTs.[52, 53] In addition, La might play a significant role in improving a catalyst lifetime.[51] Hence, La containing intermetallic alloy $LaNi_5$ was selected to take catalytic advantages to produce N–doped CNTs.

According to EDX analysis, an intermetallic compound of Ni and La originates the growth of N–doped CNTs. In shout, La might join in the synthesis process with synergic or a dual metal effect. A recent study on bimetallic catalysts for the growth of N–doped CNTs also indicate that the diffusion and solubility of C/N species were improved moderately than the sole metals, which is due to catalytic synergies.[18] Therefore, it is reasonable to speculate that the synergic effect of Ni and La catalyst provides superior solubility of C and N atoms via both surface and bulk diffusion, which leads to formation of higher nitrogen content CNTs. However, the involvement of La on the growth of N–doped CNTs is not well understood yet. Catalytic lifetime has an effective influence on the nanotubes length and the presence of La improves the

RSC Advances Accepted Manuscript

catalyst lifetime for a long duration (20 min) at the reaction temperature (900°C), as the CN/N species are diffused continuously for a whole reaction time and aids in the lengthening of the nanotubes. This is in good agreement with SEM and TEM results as shown in Fig. 2 and 6.

3.7. Effect of acid treatment on the N–content of CNTs

The effect of acid treatment on the N–content and the electronic structure of as–synthesized N–doped CNTs are also studied. It is well known that acid treatments enhance the number of defects in CNTs via facile oxidation and increases the both N–content and purity of the CNTs samples.[54, 32] So far, HNO_3 acid treatment methods on CNTs or N–doped CNTs done by boiling diluted HNO_3 acid or with a mixture of concentrated H_2SO_4 and HNO_3 for several hours.[32, 53, 56] Although, the treatment with diluted HNO_3 acid is much helpful to remove the metal content and less destructive than concentrated one.[57] In this connection, we adopted the 3M, HNO_3 and H_2SO_4 (3:1) acid mixture treatment on as–synthesized N–doped CNTs for 12 h by refluxing at 80°C.

However, we analyzed the effect of acid treatment on the N–content of as–synthesized samples by elemental analysis. In our case, we considered only change in the nitrogen content before and after purification. The N–content of as–synthesized and purified samples at different growth temperatures were listed in Table 3. The results demonstrate that the nitrogen content was slightly increased after acid treatment. The reason is due to that the carbon impurities such as amorphous carbons and graphite nanoparticles can be eliminated after acid treatment.[32] Therefore the amount of carbon content decreased, consequently nitrogen content increased slightly. The N–content of acid treated samples were 3.63, 5.79, 7.42 and 4.44 at.% for N–CNTs 800, 850, 900 and 950°C, respectively (Table 3). This result also suggests that nitrogen content of the acid treated as–synthesized samples was not varied drastically and doped to the interior of

RSC Advances Accepted Manuscript

the graphitic structure. This is consistent with the previous chemical stability investigations on N–doped CNTs as reported by Liu et al.[32]

Table 3 – N–content determination on as–synthesized and acid purified N–doped CNTs.

Growth temperature (°C)	N–content of as–synthesized samples (at.%)	N–content of acid–treated samples (at.%)
800	3.54	3.63
850	5.57	5.79
900	7.30	7.42
950	4.21	4.44

In order to identify the electronic structure of N in the acid treated sample, we performed XPS analysis. The XPS survey scan spectrum of acid treated N–doped CNTs sample (optimized condition sample, 900°C and 20 min) is shown in Fig. 14a. Compared to as–synthesized sample (Fig. 9g) the nitrogen and oxygen contents were significantly increased after acid treatment. Deconvoluted N1s XPS spectrum is shown in Fig. 14b indicates the existence of three peaks, which are located around at 398.8 eV (N1), 400.5 eV (N2) and 402.3 eV (N3), respectively. The peaks at 398.8 eV and 400.5 eV correspond to pyridine–like nitrogen and graphite–like nitrogen[16, 20, 21, 40], respectively. The peak N3 is commonly attributed to N–oxides of pyridinic–N.[39] The relative area of graphitic N, pyridinic N and N–oxides of pyridinic–N are 51.96, 26.11 and 21.93 %, respectively. The calculated atomic percentage of N in the acid treated sample was maximum of 7.3 at.%, which was quite consistent with the results of elemental analysis (Table

RSC Advances Accepted Manuscript

3). On the other hand, the proportions of graphitic N and pyridinic N decreased with significant oxygen–containing pyridinic functional groups, indicating the oxidation of nitrogen functional groups during the acid treatment. Finally, we expected that the acid treated N–doped CNTs should be potential material for electrical double layer capacitors due to increased both nitrogen and oxygen functionalities.

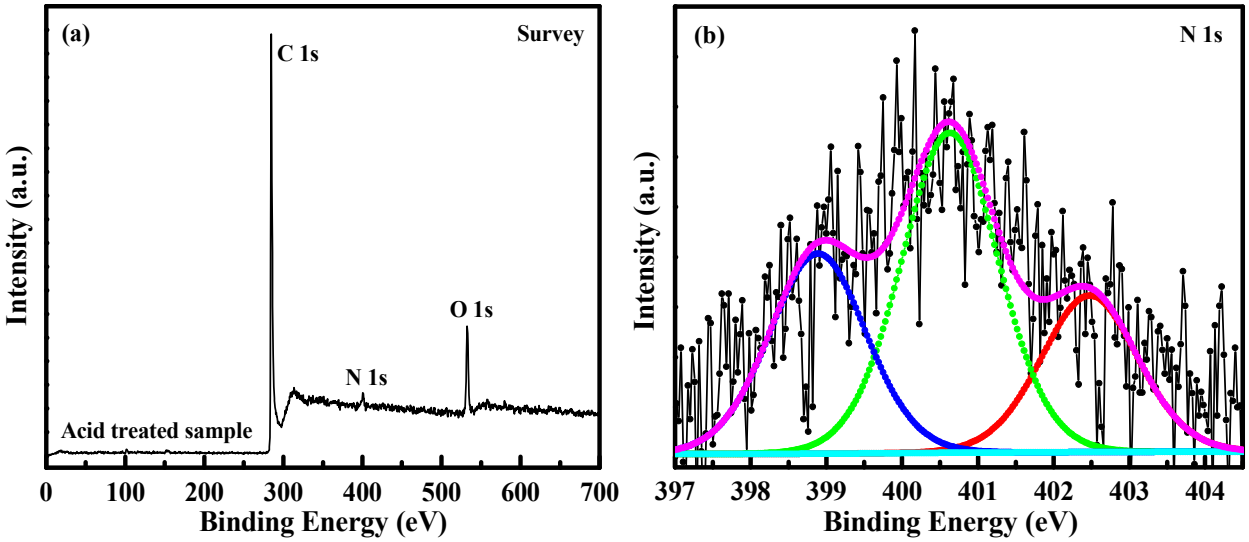

Fig. 14 – (a) and (b) XPS survey spectrum and deconvoluted N 1s spectrum of acid treated N–doped CNTs, respectively.

4. Conclusion

An alloy catalytic method was developed for the synthesis of N–doped CNTs using $LaNi_5$ catalyst by CVD from C_2H_2/NH_3 mixture. The effect of different pyrolysis temperatures and growth times on the yield, structure and C/N solubility on the alloy catalyst was carried out. The as–synthesized samples were well characterized by SEM, TEM, HRTEM, XPS and CRM. SEM and TEM results demonstrated that the increasing growth temperature and time increase the C/N solubility, diameter and the proportion of internal compartments of the nanotubes. The N–doped CNTs were synthesized at 900°C and 20 min had a high nitrogen content of 6.9 at.%. The higher

RSC Advances Accepted Manuscript

nitrogen concentration results due to the synergic effect of the intermetallic compound of Ni and La catalyst. It provides superior solubility of nitrogen through both surface and bulk diffusion and possibly helps in the formation of high nitrogen content CNTs. Acid treatment of the as–synthesized N–doped CNTs results in increased N contents with modified N environments. The final conclusion is that due to the simple synthesis procedure, higher N–doping in CNTs and N–moieties modification, it is expected that the alloy catalytic method gives promising for large scale production and various electrochemical energy storage applications such as electrical double layer capacitors, lithium–ion batteries and fuel cells.

Acknowledgements

One of the authors J. Anthuvan Rajesh is thankful to UGC, New Delhi, India for providing the Senior Research Fellowship in Sciences for meritorious students. Instrumentation facility provided under FIST–DST and DRS–UGC to Department of Chemistry and Institute of Catalysis and Petroleum Technology (ICPT), Anna University are sincerely acknowledged. The authors wish to thank Professor T. Pradeep of the DST unit of Nanoscience Indian Institute of Technology Madras for the HRTEM with EDAX analysis and Dr. Dinesh Deva research scientist of the DST unit of Nanoscience Indian Institute of Technology Kanpur for the confocal Raman spectroscopy analysis.

References

[1] K. Xiao, Y. Liu, P. Hu, G. Yu, Y. Sun and D. Zhu, *J Am Chem Soc.,* 2005, **127**, 8614–8617.

[2] K. Ghosh, M. Kumar, T. Maruyama and Y. Ando, *Carbon,* 2010, **48**, 191–200.

RSC Advances Accepted Manuscript

[3] M. Terrones, A. G. S. Filho and A. M. Rao, Doped carbon nanotubes: synthesis, characterization and applications. In: A. Jorio, G. Dresselhaus and M. S. Dresselhaus, editors. Carbon nanotubes. Topics Appl. Phys., Berlin, Heidelberg: Springer; 2008, **111**, 531–566.

[4] P. Ayala, R. Arenal, M. Rummeli, A. Rubio and T. Pichler, *Carbon,* 2010, **48**, 575–586.

[5] K. S. Lee, W. J. Lee, N. G. Park, S. O. Kim and J. H. Park, *Chem Commun.,* 2011, **47**, 4264–4266.

[6] Z. Wang, R. Jia, J. Zheng, J. Zhao, L. Li, J. Song and Z. Zhu, *ACS Nano,* 2011, **5**, 1677–1684.

[7] Z. Mo, S. Liao, Y. Zheng and Z. Fu, *Carbon,* 2012, **50**, 2620–2627.

[8] L. G. Bulusheva, A. V. Okotrub, A. G. Kurenya, H. Zhang, H. Zhang, X. Chen, H. Song, *Carbon,* 2011, **49**, 4013–4023.

[9] Y. S. Yun, H. H. Park and H.–J. Jin, *Materials,* 2012, **5**, 1258–1266.

[10] M. Glerup, J. Steinmetz, D. Samaille, O. Stephan, S. Enouz, A. Loiseau, S. Roth and P. Bernier, *Chem Phys Lett.,* 2004, **387**, 193–197.

[11] L. M. Cao, X. Y. Zhang, C. X. Gao, W. K. Wang, Z. L. Zhang and Z. Zhang, *Nanotechnology,* 2003, **14**, 931–934.

[12] M. He, S. Zhou, J. Zhang, Z. Liu and C. Robinson, *J Phys Chem B,* 2005, **109**, 9275–9279.

[13] S. K. Srivastava, V. D. Vankar, D. V. S. Rao and V. Kumar, *Thin Solid Films,* 2006, **515**, 1851–1856.

RSC Advances Accepted Manuscript

[14] A. A. Koos, M. Dowling, K. Jurkschat, A. Crossley and N. Grobert, *Carbon,* 2009, **47**, 30–37.

[15] H. Qian, A. Bismarck, E. S. Greenhalgh and M. S. P. Shaffer, *Carbon,* 2010, **48**, 277–286.

[16] J. W. Jang, C. E. Lee, S. C. Lyu, T. J. Lee and C. J. Lee, *Appl Phys Lett.,* 2004, **84**, 2877–2879.

[17] H. Chen, Y. Yang, Z. Hu, K. Huo, Y. Ma, Y. Chen, X. Wang and Y. Lu, *J Phys Chem B,* 2006, **110**, 16422–164227.

[18] H. Liu, Y. Zhang, R. Li, X. Sun and H. A. Rachid, *Particuology,* 2011, **9**, 465–470.

[19] X. Y. Tao, X. B. Zhang, F. Y. Sun, J. P. Cheng, F. Liu and Z. Q. Luo, *Diamond Relat Mater.,* 2007, **16**, 425–430.

[20] S. Y. Kim, J. Lee, C. W. Na, J. Park, K. Seo and B. Kim, *Chem Phys Lett.,* 2005, **413**, 300–305.

[21] A. G. Kudashov, A. V. Okotrub, L. G. Bulusheva, I. P. Asanov, Y. V. Shubin, N. F. Yudanov, L. I. Yudanova, V. S. Danilovich and O. G. Abrosimov, *J Phys Chem B,* 2004, **108**, 9048–9053.

[22] L. G. Bulusheva, A. V. Okotrub, A. G. Kudashov, Y. V. Shubin, E. V. Shlyakhova, N. F. Yudanov, E. M. Pazhetnov, A. I. Boronin and D. V. Vyalikh, *Carbon,* 2008, **46**, 864–869.

[23] J. P. O'Byrne, Z. Li, S. L. T. Jones, P. G. Fleming, J. A. Larsson, M. A. Morris and J. D. Holmes, *ChemPhysChem.,* 2011, **12**, 2995–3001.

RSC Advances Accepted Manuscript

[24] H. Zhang, Y. Chen, S. Li, X. Fu, Y. Zhu, S. Yi, X. Xue, Y. He and Y. Chen, *J Appl Phys.,* 2003, **94**, 6417–6422.

[25] C. M. Chen, Y. M. Dai, J. G. Huang and J. M. Jehng, *Carbon,* 2006, **44**, 1808–1820.

[26] H. Raghubanshi, M. S. L. Hudson and O. N. Srivastava, *Int J Hydrogen Energy,* 2011, **36**, 4482–4490.

[27] X. Chen, X. P. Gao, H. Zhang, Z. Zhou, W. K. Hu, G. L. Pan, H. Y. Zhu, T. Y. Yan and D. Y. Song, *J Phys Chem B,* 2005, **109**, 11525–11529.

[28] J. A. Rajesh and A. Pandurangan, *J Mater Chem C*, 2013, **1**, 6996–7008.

[29] J. A. Rajesh and A. Pandurangan, *J Nanosci Nanotechnol*., 2014, **14**, 2741–2751.

[30] C. Chen, J. Zhang, B. Zhang, C. Yu, F. Peng and D. Su, *Chem Commun*., 2013, **49**, 8151–8153.

[31] T. Fu, R. Liu, J. Lv and Z. Li, *Fuel Process Technol*., 2014, **122**, 49–57.

[32] H. Liu, Y. Zhang, R. Li, X. Sun and H. A.–Rachid, *J Nanopart Res.,* 2012, **14**, 1016 (1–8).

[33] H. J. Burch, E. Brown, S. A. Contera, N. C. Toledo, D. C. Cox, N. Grobert, L. Hao, J. F. Ryan and J. A. Davies, *J Phys Chem C,* 2008, **112**, 1908–1912.

[34] K. Jiang, A. Eitan, L. S. Schadler, P. M. Ajayan, R. W. Siegel, N. Grobert, M. Mayne, M. Reyes–Reyes, H. Terrones and M. Terrones, *Nano Lett*., 2003, **3**, 275–277.

[35] A. Zhao, J. Masa, W. Schuhmann and W. Xia, *J Phys Chem C,* 2013, **117**, 24283−24291.

[36] W. Shen and W. Fan, *J Mater Chem A*, 2013, **1,** 999–1013.

[37] J. Liu, S. Webster and D. L. Carroll, *J Phys Chem B,* 2005, **109**, 15769–15774.

RSC Advances Accepted Manuscript

[38] K. Suenaga, M. Yudasaka, C. Colliex and S. Iijima, *Chem Phys Lett.,* 2000, **316**, 365–372.

[39] K. Ghosh, M. Kumar, T. Maruyama and Y. Ando, J. *J Mater Chem.,* 2010, **20**, 4128–4134.

[40] H. C. Choi, J. Park and B. Kim, *J Phys Chem B.,* 2005, **109**, 4333–4340.

[41] D. Wei, Y. Liu, Y. Wang, H. Zhang, L. Huang and G. Yu, *Nano Lett.,* 2009, **9**, 1752–1758.

[42] A. Das, B. Chakraborty and A. K. Sood, *Bull Mater Sci.,* 2008, **31**, 579–584.

[43] R. B. Rakhi, X. Lim, X. Gao, Y. Wang, A. T. S. Wee, K. Sethupathi, S. Ramaprabhu and C. H. Sow, *Appl Phys A: Mater Sci Process,* 2010, **98**, 195–202.

[44] E. N. Nxumalo and N. J. Coville, *Materials,* 2010, **3**, 2141–2171.

[45] M. R.–Reyes, N. Grobert, R. Kamalakaran, T. Seeger, D. Golberg, M. Ruhle, Y. Bando, H. Terrones and M. Terrones, *Chem Phys Lett.,* 2004, **396**, 167–173.

[46] J. H. Yang, D. H. Lee, M. H. Yum, Y. S. Shin, E. J. Kim, C.–Y. Park, M. H. Kwon, C. W. Yang, J.–B. Yoo, H.–J. Song, H.–J. Shin, Y.–W. Jin and J.–M. Kim, *Carbon,* 2006, **44**, 2219–2223.

[47] J. Liu, H. Liu, Y. Zhang, R. Li, G. Liang and M. Gauthier, *Carbon,* 2011, **49**, 5014–5021.

[48] J. H. Yang, B. J. Kim, Y. H. Kim, Y. J. Lee, B. H. Ha, Y. S. Shin, S.–Y. Park, H. S. Kim, C.–Y. Park, C. W. Yang, J.–B. Yoo, M. H. Kwon, K. Ihm, H.–J. Song, T.–H. Kang, H.–J. Shin, Y.–J. Park and J.–M. Kim, *J Vac Sci Technol B,* 2005, **23**, 930–933.

RSC Advances Accepted Manuscript

[49] G. Y. Zhang, X. C. Ma, D. Y. Zhong and E. G. Wang, *J Appl Phys.,* 2002, **91**, 9324–9332.

[50] S. Trasobares, O. Stephan, C. Colliex, W. K. Hsu, H. W. Kroto and D. R. M. Walton, *J Chem Phys.,* 2002, **116**, 8966–8972.

[51] Q. Jiang, L. J. Song, Y. Zhao, X. Y. Lu, X. T. Zhu, L. Qian, X. M. Ren and Y. D. Cai, *Mater Lett.,* 2007, **61**, 2749–2752.

[52] Y. Saito, M. Okuda, M. Tomita and T. Hayashi, *Chem Phys Lett.,* 1995, **236**, 419–426.

[53] A. Yuliang, H. Qingyi, W. Jun, Z. Zhaohui, Z. Hui and Z. Gang, *J Rare Earths,* 2010, **28**, 717–720.

[54] E. N. Nxumalo, P. J. Letsoalo, L. M. Cele and N. J. Coville, *J Organomet Chem.,* 2010, **695**, 2596–2602.

[55] Y. C. Chiang, W. H. Lin and Y. C. Chang, *Appl Surf Sci.,* 2011, **257**, 2401–2410.

[56] F. Aviles, J. V. C.–Rodriguez, L. M.–Tah, A. M.–Pat and R. V.–Coronado, *Carbon,* 2009, **47**, 2970–2975.

[57] M. N. Tchoul, W. T. Ford, G. Lolli, D. E. Resasco and S. Arepalli, *Chem Mater.,* 2007, **19**, 5765–5772.

RSC Advances Accepted Manuscript